A search for planets transiting the M-dwarf debris disc host, AU Microscopii

Leslie Hebb,[1,2]⋆ Larry Petro,[3] Holland C. Ford,[2] David R. Ardila,[2,4] Ignacio Toledo,[5] Dante Minniti,[5] David A. Golimowski[2] and Mark Clampin[6]

[1]*School of Physics and Astronomy, University of St Andrews, North Haugh, St Andrews KY16 9SS*
[2]*Department of Physics and Astronomy, The Johns Hopkins University, 3400 North Charles Street, Baltimore, MD 21218, USA*
[3]*Space Telescope Science Institute, 3700 San Martin Drive, Baltimore, MD 21218, USA*
[4]*Spitzer Science Center, California Institute of Technology, Pasadena, CA 91125, USA*
[5]*Department of Astronomy, Pontificia Universidad Catolica de Chile, Casilla 306, Santiago 22, Chile*
[6]*NASA Goddard Space Flight Center, Code 681, Greenbelt, MD 20771, USA*

ABSTRACT

We present high-cadence, high-precision multiband photometry of the young, M1Ve, debris disc star, AU Microscopii. The data were obtained in three continuum filters spanning a wavelength range from 4500 to 6600 Å, plus Hα, over 28 nights in 2005. The light curves show intrinsic stellar variability due to star-spots with an amplitude in the blue band of 0.051 mag and a period of 4.847 d. In addition, three large flares were detected in the data which all occur near the minimum brightness of the star. We remove the intrinsic stellar variability and combine the light curves of all the filters in order to search for transits by possible planetary companions orbiting in the plane of the nearly edge-on debris disc. The combined final light curve has a sampling of 0.35 min and a standard deviation of 6.8 mmag. We performed Monte Carlo simulations by adding fake transits to the observed light curve and find with 95 per cent significance that there are no Jupiter mass planets orbiting in the plane of the debris disc on circular orbits with periods, $P \leqslant 5$ d. In addition, there are no young Neptune like planets (with radii 2.5 times smaller than the young Jupiter) on circular orbits with periods, $P \leqslant 3$ d.

Key words: circumstellar matter – stars: individual: AU Mic – stars: late-type – planetary systems – stars: pre-main-sequence.

1 INTRODUCTION

Observing planets around other stars and in various phases of their evolution is essential to understanding global properties of planetary systems and necessary for placing our own Solar System in the context of planet formation theory. The detection of a young planet of known age in which the mass and radius can be measured (i.e. a transiting planet) would provide an unprecedented empirical test of extrasolar planet models and give information on the time-scale of planetary formation. Further, the detection of a planet orbiting a debris disc star would allow investigation of the link between the planet-forming disc and the planet itself. We have initiated a project designed to address these questions by searching for transiting planets around AU Microscopii (AU Mic, GJ 803).

AU Mic is a young (∼8–20 Myr, Barrado y Navascues et al. 1999), nearby (9.94 ± 0.13pc, Perryman et al. 1997) active M-dwarf (M1Ve) star in the β Pictoris moving group which is surrounded by a nearly edge-on circumstellar debris disc (Kalas, Liu & Matthews 2004; Krist et al. 2005). Observations of substructure in the disc suggest the presence of planetary-mass bodies. Such a companion which is close to the star and orbiting in the plane of the disc would transit, causing a dip in brightness. Thus, AU Mic is an excellent target to search for transiting planets in the early stages of formation.

Our photometric monitoring campaign that is designed to detect the signature of a transiting companion orbiting AU Mic is presented in this paper. The motivation for the project is discussed in Section 2. In Section 3, the observing program, the data processing and the determination of differential photometry are explained. The results of the transit search and the parameter space in which we are sensitive to planets are described in Section 4. In Section 5, we briefly discuss the intrinsic variability of the star, and conclusions and future work can be found in Section 6.

2 AU Mic AND THE DEBRIS DISC

Direct observations of debris discs show small-scale structure, including clumps and rings of dust and gaps clear of dust (e.g. Clampin

⋆E-mail: leslie.hebb@st-andrews.ac.uk

et al. 2003; Holland et al. 2003; Weinberger, Becklin & Zuckerman 2003; Greaves et al. 2005). Orbiting planets could give rise to such substructure as planets sweep up material and gravitationally influence the dust. A large planet would produce inner gaps cleared of dust, warp asymmetries and clumps of dust at mean motion resonances (Wyatt et al. 1999; Quillen & Thorndike 2002; Wyatt & Dent 2002) that are observed in debris discs.

IRAS first detected an excess of 60-µm flux above purely photospheric emission around AU Mic, which was interpreted as circumstellar dust. Liu et al. (2004) and Chen et al. (2005) used broadband measurements between 25 and 850 µm to confirm the thermal emission from dust around the star. A single-temperature modified blackbody with temperature $T = 40 \pm 2\,\mathrm{K}$ and spectral index $\beta = 0.8$ (Liu et al. 2004) provides a good fit to the observations. In addition, recent UV measurements of molecular hydrogen absorption lines place stringent constraints on the gas–dust ratio of less than 6:1 (Roberge et al. 2005), indicating the disc is gas poor. Thus, at an age of ∼8–20 Myr most of the gas has been accreted on to the star or removed from the system, and the star no longer contains a primordial, gas-rich star-/planet-forming disc.

2.1 AU Mic disc structure

The proximity of AU Mic has allowed the debris disc to be imaged in scattered light in both optical and infrared bands, within ∼10–210 au from the star, and at resolutions as high as 0.4 au (Kalas et al. 2004; Liu 2004; Krist et al. 2005; Masciadri et al. 2005; Metchev et al. 2005). Very similar spatial features are observed independently in all the data sets, suggesting the debris disc is inclined nearly edge-on, cleared of dust in the inner regions and contains small-scale asymmetric clumps and gaps of material.

Hubble Space Telescope + ACS images show an edge-on disc with an inclination of <1° from the line of sight within 50 au of the star (Krist et al. 2005). Liu (2004) obtained images with Keck AO which resolved small-scale structures in the disc in the region from 15 to 80 au. These authors find asymmetries in the disc that cannot be explained by dust-scattering properties and thus are assumed to be structural. The disc mid-planes are unequal in length and radially confined bright and dark regions exist in both halves of the disc.

The cool dust temperature obtained through fitting the broadband spectral energy distribution (Liu et al. 2004) indicates a lack of warm dust in the inner disc near the star. According to this simple model, the 40-K dust temperature translates into an evacuated area within 17 au of the star. However, subsequent radiative transfer modelling of the scattered light finds smaller values of the disc inner radius. An evacuated area within 12 au from the star is derived by Krist et al. (2005) through modelling of the optical scattered light. Metchev et al. (2005) combine their high-resolution *H*-band AO data with the existing optical data and broad-band flux measurements to model the radiative transfer through the dust. The authors find the inner radius of the disc to be ⩽10 au. Due to the bright star, the inner edge of the disc is not directly observed in any current data set.

As observations of the debris disc surrounding AU Mic suggest the presence of large bodies, several groups have recently attempted direct detections of thermal emission from large planets at distances of 10–60 au from AU Mic using AO imaging (Masciadri et al. 2005; Metchev et al. 2005). However, no >1 Jupiter mass (M_J) planets were detected at distances >20 au from the star and no 5 M_J planets were observed beyond 10 au.
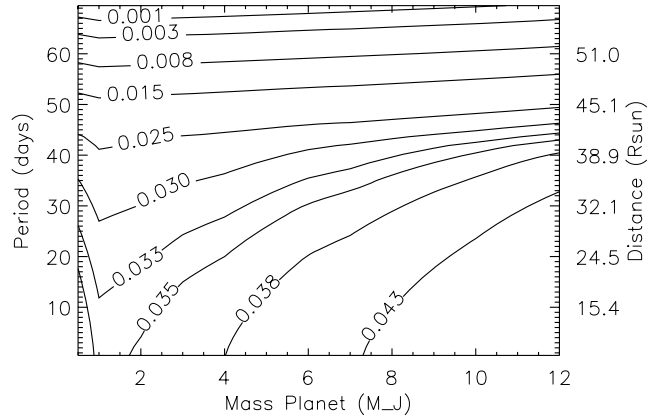

Figure 1. Contour plot of the maximum transit depth (mag) as a function of planet mass and orbital period for potential planets orbiting AU Mic. We assume the orbital plane of the planet is inclined 1° with the debris disc and adopt properties for AU Mic for a 12-Myr, $0.5\,\mathrm{M}_\odot$ star from Baraffe et al. (1998) and planet properties with masses from 0.5 to 12 M_J from Baraffe et al. (2002).

2.2 Possible transiting planets

Our group has taken a complementary approach to the search for planets around AU Mic by targeting the region <0.25 au from the star which is inaccessible with AO technology. Due to the edge-on aspect of the debris disc, close-in planets orbiting in the plane of the disc will transit the star. Adopting a 1° inclination for the disc and assuming a potential planet would orbit in the plane of the disc, we estimate the maximum period and separation at which orbiting planets will undergo transits.

Fig. 1 shows the maximum transit depth as a function of planet mass and orbital period. We take the radius for AU Mic, $R = 0.85\,\mathrm{R}_\odot$, from the stellar evolution models of Baraffe et al. (1998) for a 12-Myr, $0.5\,\mathrm{M}_\odot$ star and the planet properties from Baraffe et al. (2002) for the same age. We use the analytic transit model of Mandel & Agol (2002), which includes limb darkening, to derive the maximum transit depth. The theoretical planet radii do not vary much for planets ranging from 0.5 to 12 M_J, thus according to our simple estimates, such planets on circular orbits with periods as large as ∼70 d (orbital radius of 55 $\mathrm{R}_\odot$) will transit the star. Planets on ∼40 d orbits will undergo full, rather than grazing, transits causing dips in the light curve of >30 mmag.

3 OBSERVATIONS

3.1 Observing program

We monitored AU Mic between 2005 July 17 and August 14, with the CTIO 1-m telescope and Y4K-Cam camera. The detector consists of a 4000×4000 array of 15-µm pixels placed at Cassegrain focus giving a 0.3 arcsec pixel^{-1} plate-scale. Thus the entire array projects to a 20×20-arcmin^2 field of view. The observed signal is fed into four amplifiers causing the raw images to have a quadrant effect with the readnoise between 11 and 12 e$^-$ and gain of 1.45–1.52e$^-$/ADU, depending on the amplifier. The detector has a readout time of 51 s and a 71k-electron well depth before non-linearity sets in. This converts to a saturation of 40 000 counts pixel^{-1} in 1×1 binning mode. However, with 2×2 binning, the readout time is reduced to 16 s, and the peak binned pixel value is limited by digital saturation to 65 535 counts.

AU Mic and the surrounding field were observed in four optical filters of medium width. These include a custom filter (4520/200 Å), Stromgren-y (5497/241 Å) and Hα-off (6600/75 Å) for continuum monitoring and Hα (6563/75 Å) for activity monitoring. The Stromgren-y, Hα and Hα-off filters were available at the CTIO 1-m for use with the Y4K-Cam. An image quality 3-cavity custom filter with central wavelength $\lambda_c = 4520$ Å and width = 200 Å was ordered from Custom Scientific. The filter is $4 \times 4 \times 0.3$ in.[3] and is coated with antireflection material.

The narrow continuum filters allow us to isolate specific regions of the continuum which are free of highly variable chromospheric emission lines for optimal transit detection. The filters avoid the hydrogen Balmer lines and the Ca II H & K lines associated with chromospheric emission, as well as the strong He features at 4026, 4686 and 5875 Å, and the Na I doublet (5890 and 5896 Å) where emission peaks have been observed in absorption line cores of active M-dwarfs. In practice, the wavelength region covered by the Stromgren-y filter is shared by neutral metal lines (e.g. Fe I, Mg I, Ti I), and active M-dwarf stars are known to show very faint emission in these features during flares (e.g. Fuhrmeister, Schmitt & Hauschildt 2005; Paulson et al. 2006).

The filters provide a wide spectral coverage to aid in distinguishing non-grey star-spot variability from grey transits. In addition, the narrow filters allow us to take longer exposures that do not saturate the bright target star and that are less sensitive to instrumental systematics. Finally, we monitored in Hα to identify residual variability in our continuum light curves caused by chromospheric activity.

Throughout each observing night, we monitored in all four filters alternating between Hα and one of the continuum filters, systematically cycling through the continuum filters. We adopted 2×2 binning to obtain a faster readout time on the detector (hereafter, *pixel* refers to the binned 2×2 CCD pixel). Our observing program was designed to place the target on exactly the same detector pixels in order to minimize inaccuracies due to flat-fielding. In reality, the position of AU Mic varied within ∼5 pixel from the chosen position. Exposure times were chosen to maximize the flux in the target star and nearby reference stars while keeping the peak pixel value in AU Mic below ∼60 000 counts. We defocused the telescope to avoid saturating AU Mic while taking longer exposures to build up signal in the fainter reference stars. We monitored during non-photometric weather and changed the exposure time continuously based on the photometric transparency. Thus, exposure times were varied between 3 and 40 s in all bands. In this way, a median sampling rate of 0.8 min was obtained for Hα and ∼2.5 min for all of the continuum filters. We observed AU Mic for 6–10 h per night on 19 nights during that time. Due to poor weather, we obtained only 1–2 h of data on five nights and completely lost on additional five nights.

3.2 Processing the images

Flat-field and bias-calibration frames necessary for processing the images were obtained during each observing night. We took 2D bias frames approximately every few hours in addition to sets of biases at the beginning and end of each night. At least 10 dome flats were observed per night in all four filters, and twilight flats (3–4 per filter) were obtained when the weather was clear.

The images were processed in a standard way using routines written by L. Hebb in the IDL programming language. Before performing any processing tasks, we checked for bad frames. Images in which the peak pixel value in AU Mic is equal to 65 536 are saturated and those where the peak pixel value is less than 2000 counts have

too low transparency to obtain useful magnitude measurements of the reference stars. There were typically ∼10 out of ∼1200 such images on a full night of observing which were removed from our processing list.

Each of the four amplifiers was processed independently. All object and calibration frames were first overscan corrected (by subtracting a line-by-line median overscan value) and then trimmed. We created nightly stacked bias images by average combining all bias frames observed each night. However, we noticed a small-scale 'herringbone' pattern in the bias frames which varied over the course of an observing night. This has subsequently been observed by other groups (see http://www.lowell.edu/users/massey/obins/bias.html). The amplitude of the variability is at the level of ±10 counts pixel^{-1}, and it persists in our data. This corresponds to a maximum of 0.1 per cent of the typical AU Mic flux and 0.3 per cent of the combined flux of all the reference stars. Therefore, it contributes to the noise in the resulting light curves at the mmag level.

The stacked bias frames were subtracted from all object and flat-field images. Average combined nightly dome flats were created in each filter, and each night, the object frames and any twilight flats that were obtained were divided by the stacked dome flat. After applying the dome flat correction, there is still residual large-scale flat-field structure in the images which is stable over the course of the observing run. We tested the application of an additional illumination correction creating a stacked dome flat corrected twilight flat, and divided this image by the object images. We applied this correction to several nights of data, but it did not provide any improvement to the resulting differential photometry. This is likely because we chose reference stars within 5 arcmin of the target star over only a part of the detector in which the dome flats were a good match to the flat-field structure. As it did not improve the photometry, we did not apply this illumination correction to the data.

There is no apparent fringing structure in any of our images which span the wavelength range from 4500 to 6600 Å, including the continuum bands and Hα. Thus, we do not apply a fringe correction. In addition, the exposure times are short and the dark current is negligible. We do not apply a dark current correction as its application would only add noise to our light curves. We obtained approximately 3300 observations of AU Mic in each of the continuum filters and ∼9800 observations in Hα.

3.3 Generating light curves

3.3.1 Photometry

After the instrumental signatures were removed, source detection and aperture photometry were performed on all science frames using the Cambridge Astronomical Survey Unit (CASU) catalogue extraction software (Irwin & Lewis 2001). The software has been compared with SExtractor (http://www.ast.cam.ac.uk/~wfcam/docs/reports/simul/) and found to be very similar in the completeness, astrometry and photometry tests. The source detection algorithm defines an object as a set of contiguous pixels above a defined detection threshold. The routine requires as input the detection limit in units of background σ and the minimum number of connected pixels above that threshold which define an object. We set a detection threshold of 3σ and a minimum source size of 15 pixel, so that AU Mic, the brightest star in the field, is easily detected in all the images. Potential comparison stars up to ∼7 mag fainter are also detected.

Aperture photometry with circular apertures was performed on the detected objects in all frames. The aperture size affects the

precision of the differential photometry, thus the optimum aperture radius was chosen through empirical testing of several different sizes. An aperture which is too small will be susceptible to centring errors and can be affected by the pixelization of the detector, whereas an aperture which is too large will begin to include noise associated with sky pixels without adding much additional signal. Our experience with aperture differential photometry suggests that for bright stars, apertures larger than the median seeing produce light curves with lower rms.

The median seeing of our observations is ∼1.5 arcsec which corresponds to ∼2.6 pixels (∼1.5 arcsec). Circular apertures with radii of 2.8, 4 and 8 pixel were tested on a single night of data. The same general features are present in the light curves generated with all the tested apertures, including the intrinsic stellar variability, but the 4 pixel (2.4 arcsec) aperture produced the AU Mic light curve with the smallest scatter. Thus, we obtained instrumental magnitude measurements for all detected objects on all frames by summing the background subtracted flux contained in the 4 pixel aperture.

3.3.2 Differential photometry

To derive a differential photometry light curve for AU Mic from the instrumental photometry, we first correct for atmospheric extinction using magnitude measurements obtained on photometric nights for nearby, bright comparison stars. In each filter, we apply a linear least-squares fit to the instrumental magnitudes as a function of airmass. The derived first-order extinction coefficients are as follows: 0.21 for the 4520/200 filter, 0.14 for the 5497/245 filter and 0.083 for the 6600/75 and Hα filters. We apply these extinction corrections to all instrumental magnitude measurements. We note that this linear extinction correction is not strictly necessary since it is applied to all stars equally, and thus is removed when the differential magnitude is calculated. However, we correct for this well-understood source of flux attenuation to derive an instrumental light curve which is dominated by the fluctuating atmospheric transparency, especially as caused by thin cirrus and other clouds.

Next, we remove points from the light curves which were obtained under very poor observing conditions (>1.0 mag below the magnitude obtained under photometric conditions). In addition, we remove a handful of measurements obtained with exposure times <3 s which are adversely affected by the finite shutter opening time. Finally, we derive the differential photometry light curve for AU Mic using the measurements of 13 comparison stars within ∼5 arcmin and up to ∼5 mag fainter (in the 4520/200 band) than AU Mic.

Then we create a *super* comparison star light curve by averaging the instrumental magnitude light curves for the 13 individual stars (after subtracting the median value from each star). Initially, the 13 reference stars are weighted equally. Differential photometry light curves are then obtained for the individual comparison star light curves by subtracting the *super* light curve. Each comparison star is then assigned a weight value equal to the inverse variance of its differential photometry light curve normalized so that the weights of all 13 stars sum to one. The *super* comparison star light curve is then recreated, this time combining the individual light curves using a weighted average. The new *super* comparison star light curve is then subtracted from the instrumental AU Mic light curve. The resulting differential photometry light curves for AU Mic are shown in Fig. 2 for the four filters. Since AU Mic is significantly brighter than the nearby reference stars used to derive the differential photometry, the light-curve precision is dominated by photon Poisson noise in the reference star magnitude measurements. We have defined an error
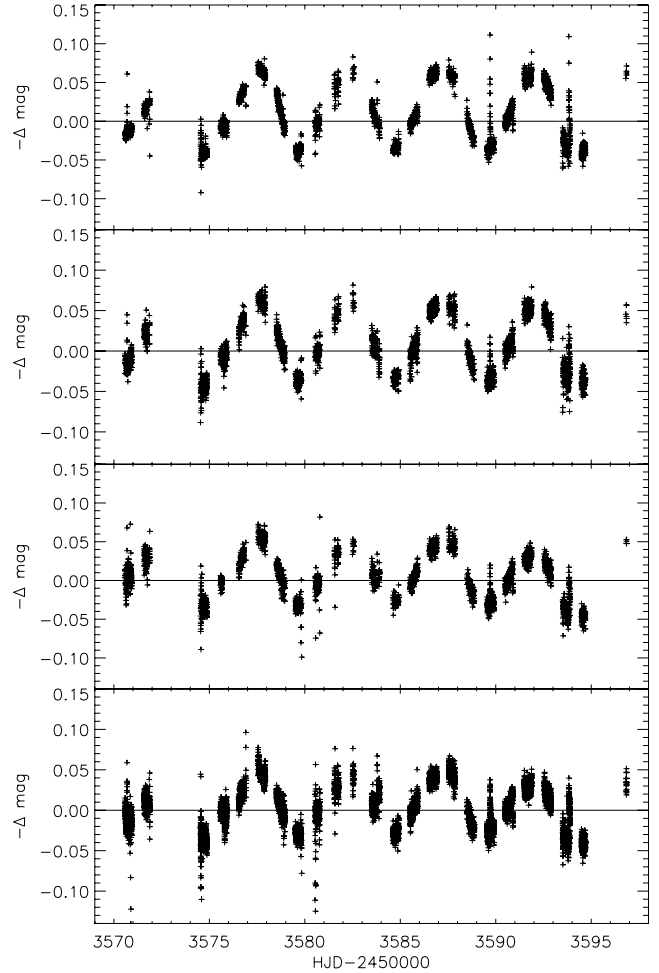

Figure 2. AU Mic differential photometry light curve in the four filters: F4520 (top), F5497 (middle-top), F6600 (middle-bottom), Hα (bottom). Star-spot variability and flaring are present in the data.

for each point on the light curve by taking the weighted standard deviation of the 13 comparison star objects used to derive that point on the AU Mic light curve.

3.3.3 Removing intrinsic variability

Fig. 2 shows the intrinsic stellar variability previously observed in AU Mic (Rodono et al. 1986). We observe flare activity and sinusoidal variability indicative of star-spots on the stellar surface. Both sources of variability are linked to magnetic activity and are typical for a young, active M-dwarf star, like AU Mic. The intrinsic variability of AU Mic is discussed briefly in Section 5. However, the variability must be removed in order to search for the signature of transiting planets in the light curve.

Both the shape and the time-scale of these sources of variability differ significantly from that of a transit, so they do not induce contamination in the transit search. During our observing campaign, three large flares occurred on AU Mic which were detected in all four filters. During the flares, the magnitude of AU Mic increased sharply within minutes and then decayed slowly to its original value over an hour to a few hours. We simply remove the regions of the AU Mic light curves which include the three large flares. Table 1 gives the range of Heliocentric Julian Dates (HJDs) which are

Table 1. HJD of flare cut-out regions.

Flare	Beginning	End
Flare 1	245 3570.68	245 3570.73
Flare 2	245 3589.69	245 3589.77
Flare 3	245 3593.82	245 3593.90

Table 2. Time-series information.

Filter	Number points	Median sampling (min)	Light curve rms (mmag)	Correlated noise (mmag)
F4520	3089	2.46	5.3	1.8
F5497	2960	2.46	7.3	1.8
F6600	2800	2.46	7.2	2.1
F6563	8737	0.70	7.6	2.3
Combined	17 593	0.35	6.8	1.7

used to exclude points from the light curve near the time of the flares.

The quasi-sinusoidal, star-spot variability occurs on time-scales of ∼5 d and varies in amplitude for the different filters. The *Hipparcos* period for this object is 4.8902 d, however we find the variation occurs on a 4.847-d time-scale (see Section 5). To remove the modulation, we experimented with fitting a truncated Fourier series to the phase-folded light curves in each filter as well as applying linear least-squares fits to the individual nights of data. We note that neither approach is a physical interpretation of the data or an attempt to model the star-spots. Both techniques produce corrected light curves with similar noise properties, thus, for this analysis, we subtract a linear fit from each night of data to produce the AU Mic light curve for each filter which is removed of intrinsic variability. Table 2 gives the number of measurements in the corrected light curve for each filter, as well as the median sampling, the rms (weighted by the error bars) and the correlated noise on a 2-h time-scale, the typical planetary transit duration. To measure the correlated noise, we calculate the rms of the light curve where each point is replaced by the average of the points in a 2-h window around that point (accounting for edge

effects) (Pont, Zucker & Queloz 2006). The rms of the smoothed light curve is 1.7 mmag which is higher than what is expected if the data were only white noise.

Since the transit signals for which we are searching will produce dips in brightness of the same depth in all four filters, we combine the four corrected light curves into a combined final AU Mic light curve, shown in Fig. 3. The combined, intrinsic variability-corrected light curve is input into the periodic transit searching algorithm. The light curve contains 17 593 points, has a median sampling of 0.35 min and has an rms of 6.8 mmag (see Table 2).

4 SEARCH FOR TRANSITING PLANETS

4.1 Systematic search for periodic transits: applying the box-least-squares algorithm

The final, combined, intrinsic variability-corrected light curve was searched for features that could have been caused by a transiting planet. We performed a systematic search for periodic, square-shaped dips in brightness using the box-least-squares algorithm of Kovács, Zucker & Mazeh (2002). We apply the algorithm to the final light curve, testing periods between 0.5 and 15 d. The short-period limit is set by the Roche radius of a Jupiter mass planet around AU Mic, and the long-period limit is approximately one-half the duration of our monitoring campaign. Known short-period, hot Jupiter planets have transit durations of a few hours, thus we search for box-shaped dips with widths corresponding to planet durations from ∼1 to 5 h.

We employ a detection statistic, which identifies the signal-to-noise ratio, S/N, of the strongest dip in brightness as a function of trial period. The signal, S, is the depth of the candidate dip, and the noise, N, accounts for both random and correlated noise (Pont et al. 2006) as both contribute significantly to the noise in our final light curve. The S/N is given by

$$\mathrm{S/N} = \frac{\mathrm{depth}}{\sqrt{\sigma^2/N_{\mathrm{intr}} + \sigma_{\mathrm{red}}^2/N_{\mathrm{tr}}^2}},$$

where 'depth' is the average depth of the transit-like event, σ is the average photometric error of the in-transit points, N_{intr} is the number of in-transit points, σ_{red} is the correlated noise on the typical transit time-scale (2 h) and N_{tr} is the number of detected transits. The
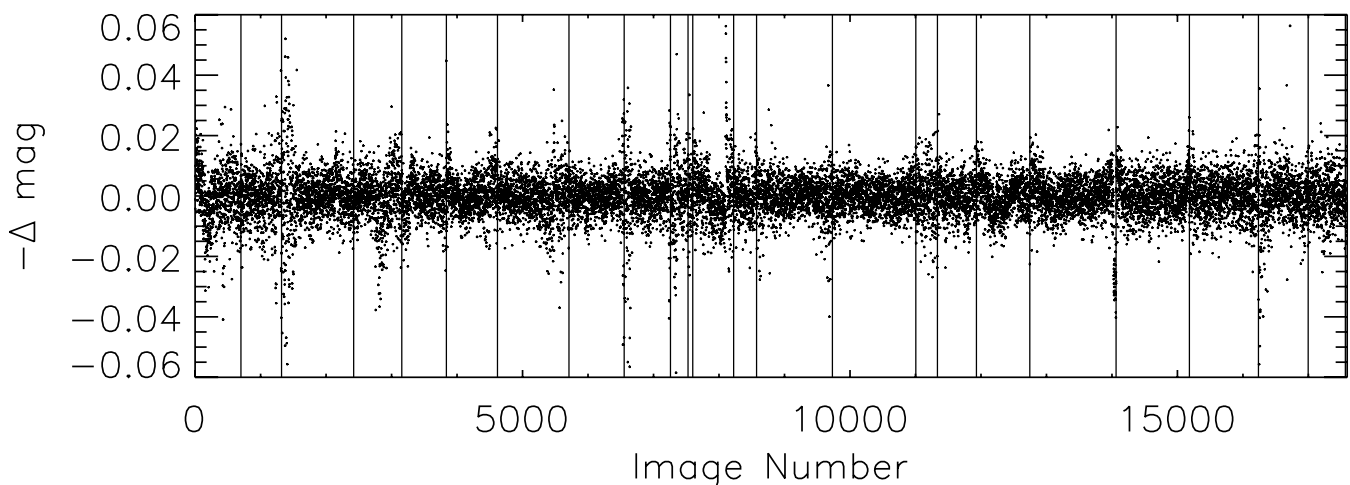

Figure 3. Combined, intrinsic variability-corrected, differential photometry light curve of AU Mic plotted versus image number. The data contain differential magnitudes for all four filters. They are removed of flares and corrected for the rotationally modulated star-spot brightness. The vertical lines are placed at the positions of the night breaks.

resulting periodogram (S/N versus trial period) was then examined for significant peaks which would indicate periodic box-shaped dips in the light curve. We set a threshold of S/N = 8.8 to define a significant detection.

The detection threshold of S/N = 8.8 was derived from analysing a set of simulated light curves which contained only noise (no fake transits). We generated a set of 400 fake light curves with the same window function and noise properties of the observed light curve. This allows structure in the periodogram which arises due to the window function to mimic that of the observed light curve. The delta magnitude values are different for each simulated light curve and consist of the sum of a red noise component and a white noise component. The noise in each simulated light curve is randomly determined using the measured values given in Table 2.

The 400 simulated light curves, including only noise, were searched for transits in the same fashion as the observed data. We applied the box-fitting algorithm to each light curve and measured the peak S/N value that was detected. The algorithm typically finds a low-level spurious signal with a depth of $\sim$2 mmag and an S/N $\sim$ 6 in the simulated data. For the ensemble of simulated light curves, the distribution of output S/N values has a mean of 6.1 and a σ of 0.9. 99.7 per cent (3σ) of the simulated light curves produce a peak S/N < 8.8, so we adopt this value as the detection threshold to define significant periodic transits in the real data.

4.2 Detection and analysis of event: is it caused by a transiting planet?

The periodogram resulting from the periodic transit search on the intrinsic variability corrected AU Mic light curve is shown in Fig. 4. There are many peaks in the periodogram above the significant detection level of S/N = 8.8. From this, we infer that a significant box-shaped dip in brightness is present; however, a unique period is not identified for it. Only one dip is apparent in a close visual inspection of the light curve, and the multiple peaks in the periodogram are likely due to the single event aliasing with the window function.

The single observed dip in brightness occurs in all four filters during the last 20 min of night JD 245 3590. It consists of 39 data points, beginning at HJD = 245 3590.884 766 and continuing until the observation is stopped for the night at HJD = 245 3590.898 682. The average depth is 26.4 mmag, resulting in an S/N = 10.0. Fig. 5 shows a blow-up of the light-curve region which includes the transit-like event. The dip is clearly shown and is highly significant, however, it is not repeated, the ingress is very sudden, and the egress is not
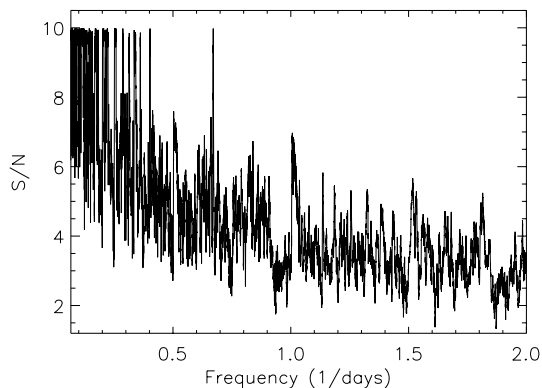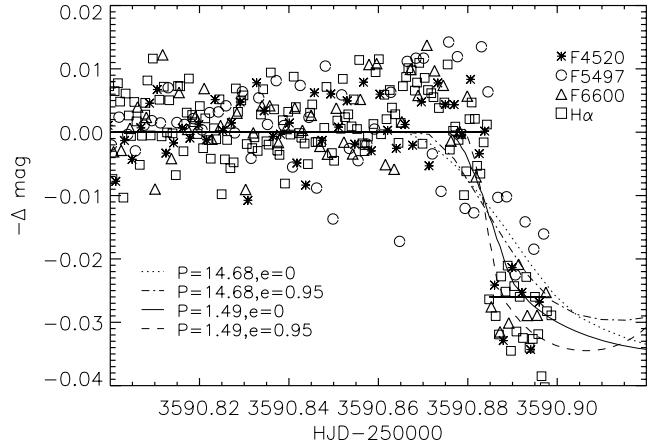
Figure 5. Light curve of AU Mic zoomed-in on the detected dip in brightness. The data from the four filters are shown as different symbols (F4520, asterisks; F5497, circles; F6600, triangles; Hα, squares). Four transit model light curves from Mandel & Agol (2002) are overplotted. The model light curves correspond to planets with orbital periods and eccentricities of: P = 1.49 d, e = 0.0 (solid), P = 1.49 d, e = 0.95 (dashed), P = 14.48 d, e = 0.0 (dotted), and P = 14.48 d, e = 0.95 (dot–dashed). We adopt a stellar radius of R = 0.85 R$_\odot$ (12-Myr, 0.5 M$_\odot$ star (Baraffe et al. 1998) and a planet radius of 0.13 R$_\odot$ to roughly reproduce the depth of the dip.

observed. Therefore, it is possible the dip is due to an instrumental, rather than astrophysical cause.

4.2.1 Considering instrumental explanations

We first examined the light curves of the individual reference stars for the night of JD 245 3590. The reference stars showed no sudden brightness variations at the end of the night which would have caused the observed dip in the differential magnitude of AU Mic. We then checked for trends in the AU Mic light curve with instrumental properties. We plotted the data against the peak counts in AU Mic and its position on the detector, but found no correlation with the observed dip. On the same night, we checked for a relationship between the differential magnitudes and their corresponding airmasses, exposure times, background levels and seeing measurements. Again, we found no correlation between these instrumental properties and the differential photometry which could have caused the drop in brightness. In addition, we tested several photometric aperture sizes, and all showed the same dip in the light curve with the same depth and timing. Thus, we identified no systematic instrumental cause for the dip. However, its nature is still uncertain. To determine whether the drop in brightness could have been caused by a transiting planet, we investigate the type of planet that would be required to be consistent with the observed light curve.

4.2.2 Depth and period constraints

If a transiting planet caused the observed dip in brightness, it would have to be quite large. The relationship between transit depth and planet radius can be approximated by depth $\sim 1.3 \times (R_p/R_s)^2$ (Tingley & Sackett 2005). Given a measured depth of 26.4 mmag and adopting a radius for AU Mic of 0.85 R$_\odot$ (Baraffe et al. 1998), the planet radius is found to be $R_p \sim 1.1$ Jupiter radii. Although there are large uncertainties in the stellar evolution models used to define the stellar radius, and the depth equation is an approximation

Figure 4. Periodogram resulting from the box-fitting algorithm.

which is strictly only valid in the *I* band, it is clear that only a planet with a Jupiter like radius could account for the observed dip.

A transiting planet should show multiple dips in brightness occurring at periodic intervals. This was not observed. However, due to the window function of the light curve, it is possible that additional events occurred while we were not observing (e.g. during daytime or poor weather). Therefore, there are only certain periods between 0.5 and 15 d which are consistent with a transiting planet as the cause for the observed event. Peaks in the periodogram identify potential periods, which all have identical S/N values because they identify the same dip in brightness. The shortest possible transiting planet periods which are still consistent with the data are $P = 1.492$, 2.484 and 3.870 d. The number of such periods increases with orbital period, with the longest one (within our search range) being $P = 14.680$ d. Although, we are not sensitive to periodic signals longer than the duration of our observing campaign, we note that many possible planet periods outside our search range, between 15 and 70 d (see Section 2.2), are also possible.

4.2.3 *Constraints from the ingress*

The observed dip in brightness is very sharp with little or no apparent ingress. To determine whether a planet could cause such a sharp transit, we compared the observed dip to model light curves from Mandel & Agol (2002). Four model light curves which represent the extremes of the potential planets and which are consistent with the depth and period constraints defined above are overplotted on the data in Fig. 5. Both the planet period and eccentricity affect the shape and duration of the ingress (if the depth of the transit and radius of the star are fixed), thus we try two different orbital periods of $P = 1.49$ and 14.68 d, which both correspond to peaks in the periodogram. For both periods, we show the ingress curve of a planet with an eccentricity of $e = 0.0$ and 0.95 to represent the extremes at each period. We adopt a stellar radius, $R_{\rm s} = 0.85\,{\rm R}_\odot$, for a 12-Myr, $0.5\,{\rm M}_\odot$ star (Baraffe et al. 1998) and a planet radius, $R_{\rm p} = 0.13\,{\rm R}_\odot$, which is consistent with a Jupiter mass planet of this age and roughly reproduces the depth of the feature in the observed light curve. A quadratic limb-darkening law is used with parameters found in Claret (2000) for a star with $T_{\rm eff} = 3500\,{\rm K}$ and $\log g = 4.0$.

The long-period planet models ($P = 14.68$ d) shown here are inconsistent with the data due to their relatively long ingress compared to the sharpness of the observed dip. Consequently, planets on longer period orbits would also be unable to explain the data. The short-period planet ($P = 1.49$ d) on a circular orbit ($e = 0.0$) is also largely inconsistent with the observed sharpness of the dip. The ingress of the short-period planet on the highly eccentric orbit provides the closest match to the shape of the dip; however, it still does not replicate the sharpness of the observed feature.

In summary, we placed constraints on the properties of a potential orbiting planet that could have caused the drop in brightness of AU Mic that was observed on JD 245 3590. The combination of the deep, sharp, non-repeated dip makes it unlikely that the observed feature, shown in Fig. 5, was caused by a transiting planet. In addition, there is no reason for us to believe the feature is caused by an instrumental problem. Therefore, we conclude this single event which mimics a planetary transit is unexplained, and additional data are required to determine its true nature.

4.3 Search for smaller planets

In order to search for smaller planets in the data, we first remove the dip in brightness discussed in Section 4.2 by subtracting the aver-

age depth of the dip (26.4 mmag) from the data points between HJD = 245 3590.884 766 and 245 3590.898 682. We then rerun the box-fitting algorithm. In this trial, the highest peak in the periodogram has an S/N = 6.4, and thus is only consistent with noise. Therefore, we do not detect any significant, low-amplitude periodic box-shaped dips in brightness. The implications of this non-detection are discussed below.

4.4 Fake transit simulations

To set limits on the type of planet which could have been detected in our data, we generated simulated light curves with fake transits added to the observed data and tried to recover the transit signal.

In the simulations, we placed a planet in orbit around AU Mic in the plane of the debris disc (inclination angle equal to 1° from the line of sight). We adopted a host star radius of $0.85\,{\rm R}_\odot$ for a 12-Myr, $0.5\,{\rm M}_\odot$ star. The orbital phase of the simulated planet was chosen randomly from a uniform distribution, and the orbital period of the planet was chosen randomly from a uniform distribution within our search range (0.5–15 d). All simulated planets are assumed to be on circular orbits. We made no attempt to adopt the distribution of orbital properties of known planets since there are no observed data to constrain these values at the age of AU Mic. Noise-free model light curves were created using the analytic eclipse models of Mandel & Agol (2002) which were then added to a version of the observed data in which the detected dip in brightness described in Section 4.2 was subtracted off. Thus, the simulated light curves with fake transits added have the same noise properties and sampling as the observed light curve.

The fake transit light curves were run through the box-fitting algorithm using the same search parameters as the observed data (searching for periods between 0.5 and 15 d and durations of ∼1– 5 h). The fake transits were considered recovered if the transit signature was detected with an S/N $\geqslant 8.8$ and the derived period was within 5 per cent of the input orbital period. Alias periods which are one-half or twice the input period are also considered recoveries.

We ran two sets of simulations (with 400 light curves each) using two different planet radii. First, we simulated a $1\,M_{\rm J}$ planet in orbit around AU Mic adopting radius, $R_{\rm p} = 0.134\,{\rm R}_\odot$ for a 12-Myr, $1\,M_{\rm J}$ planet from Baraffe et al. (2002). Such a planet produces an unmistakable signal in the simulated light curves with a depth of >30 mmag. The recovery fraction is a strong function of input period, as is shown in Fig. 6 which plots the fraction of transiting Jupiter mass planets detected in the simulations as a function of input orbital period. If we consider only short-period planets with periods, $P \leqslant 5$ d, 99 per cent of the sample are significant detections with an S/N > 8.8 (solid line in Fig. 6), and for 95 per cent, the period is also correctly recovered (dashed line).

We ran an additional set of simulations using a planet which represents a possible Neptune like planet at the age of AU Mic. Since the theoretical models do not reach the mass of Neptune and no young Neptune mass planets have been observed, we simply adopt a mass, $M = 0.05\,{\rm M}_\odot$, and a radius, $R = 0.054\,{\rm R}_\odot$, which is 2.5 times smaller than the radius of the 12-Myr-old Jupiter. This type of planet produces a transit depth of ∼5 mmag which is smaller than the noise limit of the data. However, for orbital periods, $P \leqslant 3$ d, 95 per cent of the simulated transit light curves are detected with an S/N > 8.8. In 92 per cent of the cases, the period is also recovered. Fig. 7 shows a plot of the fraction of transiting Neptune like planets detected in the simulations as a function of orbital period.
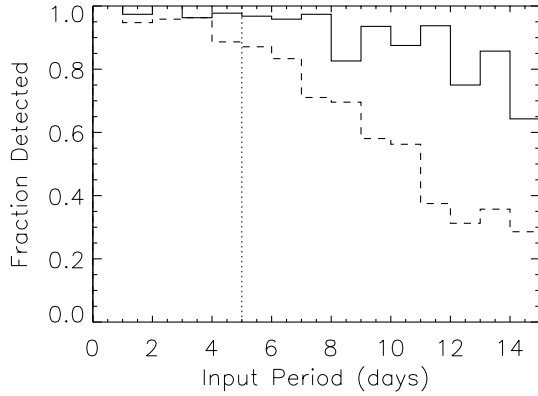
Figure 6. Fraction of simulated Jupiter mass planets detected in the fake transit Monte Carlo simulations as a function of input orbital period. The solid line shows the fraction detected with an S/N > 8.8, and the dashed line shows the recovery fraction with an S/N > 8.8 and in which the period found by the box-fitting algorithm is within 5 per cent of the input period (including twice and one-half aliases) (dashed line). The vertical dotted line corresponds to the 5 d period limit which is discussed in Section 4.4.
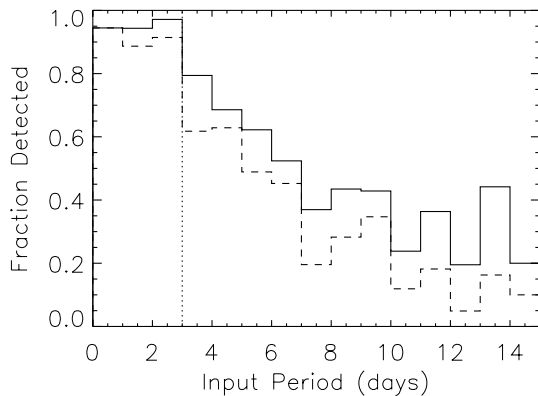

Figure 7. Results of the fake transit Monte Carlo simulations. Fraction of simulated Neptune like planets, with a mass, $M = 0.05 M_J$, and a radius, $R = 0.054 \, R_\odot$, which is 2.5 times smaller than the radius of the 12-Myr-old Jupiter. The solid line shows fraction detected with an S/N > 8.8, and the dashed line shows the recovery fraction with an S/N > 8.8 and in which the period found by the box-fitting algorithm is within 5 per cent of the input period (including twice and one-half aliases) (dashed line). The vertical dotted line corresponds to the 3 d period limit which is discussed in Section 4.4.

4.5 Interpretations

We interpret the results of the transit search on the observed light curve in the context of the fake transit simulations. Due to the lack of a convincing planetary transit detection in our observed light curve, we find, with 95 per cent confidence, that there are no Jupiter mass planets on circular orbits around AU Mic with periods ⩽5 d. We find at the 92 per cent confidence level that there are no young planets with smaller radii (Neptune like) orbiting AU Mic on circular orbits with periods ⩽3 d.

It is important to note that the Monte Carlo simulations described above are based on theoretical stellar evolution models which are uncalibrated and untested by observations for low-mass stars and planets at the young age of AU Mic (Aigrain et al. 2007). In addition, early M-dwarfs are rapidly evolving in radius between 10 and 20 Myr, therefore, uncertainties in the age of AU Mic will produce uncertainties in the results of our simulations.
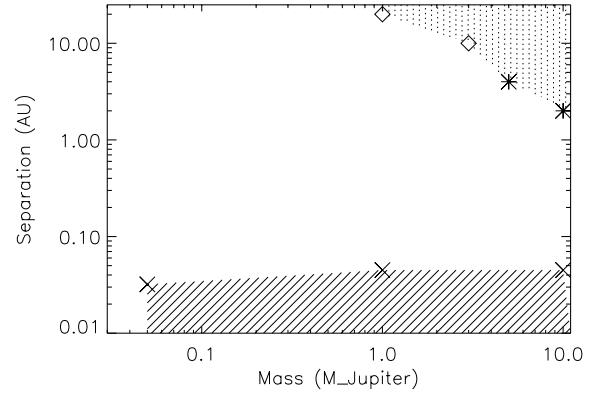

Figure 8. Region of planet parameter space as a function of planet mass and orbital separation showing the constraints on the existence of planets around AU Mic given by adaptive optics from Metchev et al. (2005, diamonds) and Masciadri et al. (2005, asteriks) and time-series photometry (this work, crosses). The hashed areas show regions of the mass/separation parameter space in which the existence of a planet is ruled out with high significance.

We combine our results with the constraints placed by adaptive optics imaging (Masciadri et al. 2005; Metchev et al. 2005) on the existence of planets orbiting in the outer parts of the AU Mic disc. In Fig. 8, we show the region of parameter space as a function of planet mass and orbital separation in which an existing planet would have been detected. The existence of a planet in the hashed region of the diagram is ruled out with high significance due to the lack of a secure planet detection in either the adaptive optics or the photometric monitoring data set. There is still a large region of parameter space left to be explored. The search for transiting planets can potentially explore beyond the existing constraints out to 0.25 au. Radial velocity measurements should be able to detect planets in the system out to several au; however, the stellar activity will reduce the detection sensitivity of this method.

5 INTRINSIC STELLAR VARIABILITY

In addition to the planet search, the high-cadence, multiband photometric data set described in this paper provides information about the intrinsic variability of AU Mic. We briefly report on the findings, but save a more in-depth discussion, analysis and modelling for a future paper.

5.1 Star-spot variations

The stellar variability due to star-spots is quasi-sinusoidal and periodic on the time-scale of the stellar rotation period. We measure the periodicity in the light curve using a Lomb–Scargle periodogram (Scargle 1982) combining data from all the filters. The main peak in the periodogram is highly significant and occurs at 4.847 d. Our data cover approximately six rotations of the star; however with a period very close to 5 d, the phase coverage is incomplete. The period we derive is closer to the 4.854 d period found by Torres, Mello & Quast (1972) than to the *Hipparcos* period of 4.8902 d.

The amplitude of the variability is a function of passband, indicating the wavelength dependence of the flux of the cool star-spots causing the variability. Adopting our derived period, we perform a linear least-squares fit of the phase-folded light curve with respect to a sine function to determine the amplitude of the initial Fourier mode. The amplitude of the variability is 0.051, 0.047 and 0.039 mag in the F4520, F5497 and F6600 filters. The Hα band shows a
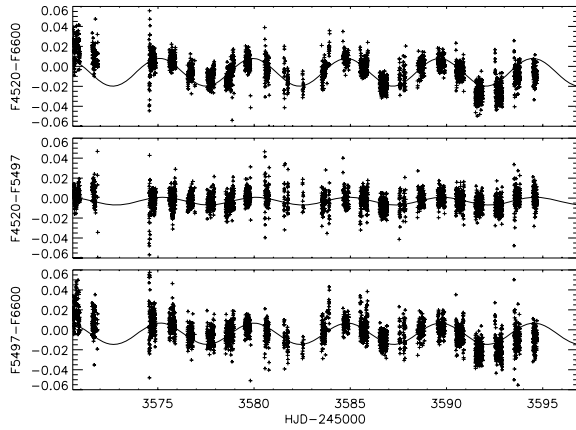
Figure 9. Light curves of the colours of the star-spot variations: F4500–F6600 (top), F4500–F5497 (middle) and F5497–F6600 (bottom). Sine wave fits to the data are overplotted adopting the $P = 4.847$ d period of the modulation.

0.035 mag amplitude variability. The decrease in amplitude with wavelength is expected if the majority of star-spots are cooler than the stellar photosphere. Fig. 9 shows the colours of the variability emphasizing the change in amplitude of the modulation with wavelength.

5.2 Flare activity

We report the detection of three large optical flares, observed in all four filters, during the month-long monitoring campaign of AU Mic. Three of our filters show flaring of the continuum of the star; the Hα filter represents the chromospheric activity. The observed flares show the characteristic structure of a rapid rise time and slower decay. They tend to occur when the star is near the minimum of the light curve which suggests they emanate from the most heavily spot covered hemisphere of the star. This has been observed in T Tauri flare stars such as V410 Tau (Fernández et al. 2004). Magnetic fields impede convection on the photosphere giving rise to star-spots, thus it is not surprising that the flares, caused by magnetic activity, are associated with the heavily covered hemisphere of the star. A close-up of the light-curve flare regions are shown in Fig. 10.

We have measured the peak amplitude of the flares in each filter, as well as the rise time and exponential decay time-scale. The values are found in Table 3. The continuum filters show increasing amplitude
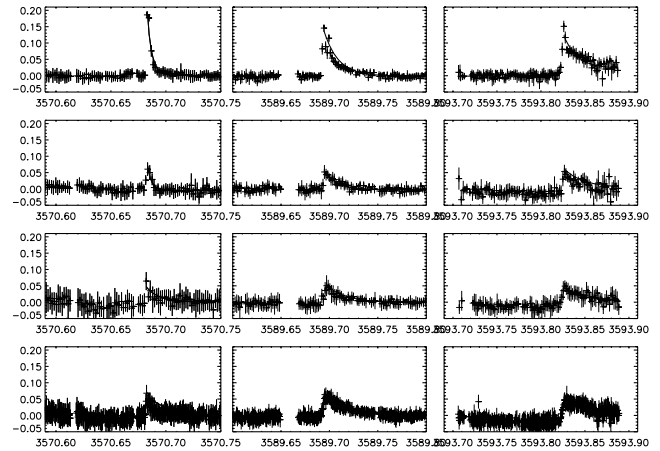

Figure 10. Regions of the light curves including the three flares observed flares. Flare 1 is shown in the left-hand column F4500 (top), F5497 (second from top), F6600 (second from bottom) and Hα (bottom) filters. Flare 2 is in the middle column, and Flare 3 is in the right-hand column. The best-fitting exponential models to the decaying part of each flare are overplotted.

with decreasing wavelength. We resolve the rise time of the flare in Hα, but not in any of the other filters due to our higher Hα sampling rate. However, the data suggest the faster the rise time of the flares, the faster the decay time-scale. In addition, the shorter wavelength observations tend to show faster rise and decay time-scales. Finally, there appears to be pre-flare absorption in the Hα light curve which is most prominent before the first flare.

6 CONCLUSIONS AND FUTURE WORK

We have obtained unprecedented high-cadence, high-precision photometry of the young, M1Ve, debris disc star, AU Mic in four medium band filters over 28 nights. The combined light curve has a sampling rate of less than 1 min and an rms (when the intrinsic stellar variability is removed) of 6.8 mmag. The light curve was searched for transiting extrasolar planets by applying a box-fitting algorithm designed to detect grey (same depth in all filters), periodic, square-shaped dips in brightness. We detected one significant event S/N =10.0 which occurred at the end of the night in all four filters with a depth ∼26.4 mmag. However, the constraints placed by the depth, period and shape of the observed dip suggest that it is unlikely to be caused by a transiting planet. More data are required

Table 3. Flare properties.

Flare	Filter	Start time	Rise time (min)	Exponential decay time-scale (min)	Peak exponential fit (mag)	Peak delta magnitude (mag)
1	F4520	3570.680 91	<2.8	6.2	0.195	0.183
1	F5497	3570.679 93	2.5–4.9	5.3	0.076	0.063
1	F6600	3570.680 42	<2.5	15.6	0.046	0.065
1	Hα	3570.681 40	0.7–1.4	26.5	0.064	0.070
2	F4520	3589.690 92	2.5–4.9	21.3	0.138	0.147
2	F5497	3589.691 65	2.1–4.6	20.4	0.054	0.053
2	F6600	3589.690 43	7.0–9.5	27.6	0.052	0.053
2	Hα	3589.691 89	3.9–4.6	29.3	0.066	0.066
3	F4520	3593.819 09	7.4–9.8	22.1	0.101	0.150
3	F5497	3593.823 00	2.5–5.3	30.8	0.056	0.064
3	F6600	3593.820 07	7.7–10.2	61.5	0.047	0.055
3	Hα	3593.822 75	4.2–5.3	33.5	0.052	0.052

to determine its nature. Therefore, in the observed light curve, we find no convincing transit events which could be caused by a planet orbiting AU Mic.

We performed Monte Carlo simulations by adding fake transits to the light curve to determine the probability of detecting a planet around AU Mic given the window function and noise properties of our data. The signature of a young Jupiter mass planet on a short-period orbit would be easily detected. The results of the simulations indicate there are no planets with masses, $M > 1\,M_J$ orbiting AU Mic in the plane of the debris disc ($\sim 1°$) with periods, $P < 5$ d. A young Neptune like planet with a smaller radius ($2.5 \times$ smaller than the young Jupiter) could also be detected in our data. The lack of such a detection indicates there are no young Neptune like planets orbiting AU Mic with periods, $P < 3$ d.

In addition to the transit search, the high-cadence, multiband photometry is ideal for examining the intrinsic stellar variability of the star due to star-spots and flaring activity. AU Mic exhibits quasi-sinusoidal variability likely due to an uneven distribution of star-spots on the stellar surface. The amplitude of the variability varies from 0.051 mag in the blue to 0.039 mag in the red. Using the periodic modulation, we derive a stellar rotation period for the star of 4.847 d. We also report on the detection of three large optical flares which tend to emanate from the most heavily spotted hemisphere of the star. A more in-depth analysis and modelling of the intrinsic stellar variability will be discussed in a subsequent paper.

New observations that were obtained in 2006 August and September using the CTIO 1-m and Australian National Universty (ANU) 40-in. telescopes will help place further constraints on the existence of planets around AU Mic and allow improved modelling of the intrinsic stellar variability.

ACKNOWLEDGMENTS

REFERENCES

Aigrain S., Hodgkin S., Irwin J., Hebb L., Irwin M., Favata F., Moraux E., Pont F., 2007, MNRAS, 375, 29

Barrado y Navascués D., Stauffer J. R., Song I., Caillaut J.-P., 1999, ApJ, 520, L123
Baraffe I., Chabrier G., Allard F., Hauschildt P. H., 1998, A&A, 337, 403
Baraffe I., Chabrier G., Allard F., Hauschildt P. H., 2002, A&A, 382, 563
Chen C. H. et al., 2005, ApJ, 634, 1372
Clampin M. et al., 2003, AJ, 126, 385
Claret A., 2000, A&A, 363, 1081
Fernández M. et al., 2004, A&A, 427, 263
Fuhrmeister B., Schmitt J. H. M. M., Hauschildt P. H., 2005, A&A, 439, 1137
Greaves J. S. et al., 2005, ApJ, 619, L187
Holland W. S. et al., 2003, ApJ, 582, 1141
Irwin M., Lewis J., 2001, New Astron. Rev., 45, 105
Kalas P., Liu M. C., Matthews B. C., 2004, Sci, 303, 1990
Kovács G., Zucker S., Mazeh T., 2002, A&A, 391, 369
Krist J. E. et al., 2005, AJ, 129, 1008
Liu M., 2004, Sci, 305, 1442
Liu M. C., Matthews B. C., Williams J. P., Kalas P. G.2004, ApJ, 608, 526
Mandel K., Agol E., 2002, ApJ, 580, L171
Masciadri E., Mundt R., Henning T., Alvarez C., Barrado y Navascués D., 2005, ApJ, 625, 1004
Metchev S. A., Eisner J. A., Hillenbrand L. A., Wolf S., 2005, ApJ, 622, 451
Paulson D. B., Allred J. C., Anderson R. B., Hawley S. L., Cochran W. D., Yelda S., 2006, PASP, 118, 227
Perryman M. A. C. et al., 1997, ESA SP-1200, The Hipparcos and Tycho Catalogues. ESA Publications Division, Noordwijk
Pont F., Zucker S., Queloz D., 2006, MNRAS, 1146
Quillen A. C., Thorndike S., 2002, ApJ, 578, L149
Roberge A., Weinberger A. J., Redfield S., Feldman P. D., 2005, ApJ, 626, L105
Rodono M. et al., 1986, A&A, 165, 135
Scargle J. D., 1982, ApJ, 263, 835
Strom S. E., Edwards S., 1993, ASP Conf. Ser. Vol. 36, Planets Around Pulsars, p. 235
Tingley B., Sackett P. D., 2005, ApJ, 627, 1011
Torres C. A. O., Mello S. F., Quast G. R., 1972, ApJ, 11, L13
Weinberger A. J., Becklin E. E., Zuckerman B., 2003, ApJ, 584, L33
Wyatt M. C., Dent W. R. F., 2002, MNRAS, 334, 589
Wyatt M. C., Dermott S. F., Telesco C. M., Fisher R. S., Grogan K., Holmes E. K., Piña R. K., 1999, ApJ, 527, 918

This paper has been typeset from a TeX/LaTeX file prepared by the author.